ACS APPLIED MATERIALS & INTERFACES

Letter

www.acsami.org

Ultraviolet Electroluminescence from Nitrogen-Doped ZnO-Based Heterojuntion Light-Emitting Diodes Prepared by Remote Plasma in situ Atomic Layer-Doping Technique

Jui-Fen Chien,[†] Hua-Yang Liao,[‡] Sheng-Fu Yu,[§] Ray-Ming Lin,[⊥] Makoto Shiojiri,[#] Jing-Jong Shyue,[†,‡] and Miin-Jang Chen*[,†,‖]

[†]Department of Materials Science and Engineering, National Taiwan University, Taipei 10617, Taiwan, Republic of China

[‡]Research Center for Applied Sciences, Academia Sinica, 128 Sec. 2, Academia Road, Nankang, Taipei 11529, Taiwan

[§]Institute of Microelectronics, Department of Electrical Engineering, National Cheng Kung University, Tainan 70101, Taiwan

[⊥]Graduate Institute of Electronic Engineering and Green Technology Research Center, Chang Gung University, Taoyuan 333, Taiwan

[#]Kyoto Institute of Technology, Kyoto 606-8585, Japan

[‖]National Nano Device Laboratories, Hsinchu 30078, Taiwan

ABSTRACT: Remote plasma in situ atomic layer doping technique was applied to prepare an *n*-type nitrogen-doped ZnO (*n*-ZnO:N) layer upon *p*-type magnesium-doped GaN (*p*-GaN:Mg) to fabricate the *n*-ZnO:N/*p*-GaN:Mg heterojuntion light-emitting diodes. The room-temperature electroluminescence exhibits a dominant ultraviolet peak at $\lambda \approx 370$ nm from ZnO band-edge emission and suppressed luminescence from GaN, as a result of the decrease in electron concentration in ZnO and reduced electron injection from *n*-ZnO:N to *p*-GaN:Mg because of the nitrogen incorporation. The result indicates that the in situ atomic layer doping technique is an effective approach to tailoring the electrical properties of materials in device applications.

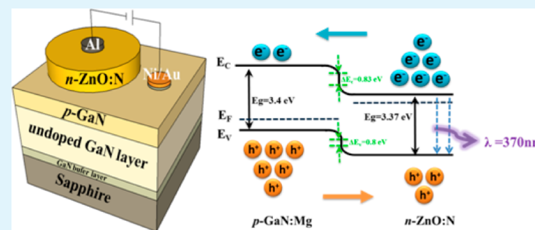

KEYWORDS: *atomic layer deposition, zinc oxide, heterojunction, light-emitting diode, remote plasma, in situ atomic layer doping*

■ INTRODUCTION

The short-wavelength light-emitting diodes (LEDs) have been widely applied in solid-state lighting, backlight modules, and laser diodes.[1,2] Among the short-wavelength materials, ZnO has attracted considerable attention because it has many benefits, such as large exciton binding energy up to 60 meV, low material cost, compatibility with wet chemical etching, environmental friendliness, and biocompatibility. Nevertheless, as of now it is still difficult to produce reliable and high-quality *p*-type ZnO. Because ZnO and GaN have the same crystal structure (würtzite) and a small in-plane lattice mismatch (1.8%), *p*-type GaN has been considered to substitute for *p*-type ZnO. Therefore, *n*-ZnO/*p*-GaN heterojunction LEDs have been developed, in which the *n*-ZnO layers were prepared using plasma-assisted molecular beam epitaxy,[3] RF sputter,[4,5] metal—organic chemical vapor deposition,[6,7] pulse laser deposition,[8,9] and atomic layer deposition.[10,11] However, most of the *n*-ZnO/*p*-GaN heterojunction LEDs reported in the literatures exhibited the electroluminescence (EL) spectra in the blue spectral region,[3,12−14] indicating that the radiative carrier recombination mainly takes place in the *p*-GaN layer. It might result from the dominant electron injection from *n*-ZnO over the hole injection from *p*-GaN because of the much higher carrier concentration in *n*-ZnO than the hole concentration in *p*-GaN.

In this work, we used atomic layer deposition (ALD) to prepare an *n*-type nitrogen-doped ZnO (*n*-ZnO:N) layer on *p*-type magnesium-doped GaN (*p*-GaN:Mg) to fabricate the *n*-ZnO:N/*p*-GaN:Mg heterojunction LEDs. ALD utilizes surface-controlled chemical reactions for depositing materials with atomic-layer accuracy. As compared with other thin-film deposition techniques, the advantages of ALD include accurate thickness and composition control, excellent conformality and step coverage, high uniformity over a large area, low defect density, and good reproducibility. Besides, ALD has the in situ atomic layer doping capability of achieving a high dopant concentration and maintaining atomic level control of the doping process because of the self-limiting and layer-by-layer (or "digital") growth. Actually, ZnO:N thin films have been demonstrated by the in situ atomic layer doping technique in our previous work.[15] The nitrogen concentration can be precisely controlled by the number of atomic doped layers, clearly indicating that the in situ atomic layer doping technique is a well-controlled process. The X-ray photoelectron and X-ray absorption near edge spectroscopies revealed the formation of N-related acceptor states due to the occupation of O sites with

Received: August 27, 2012
Accepted: December 21, 2012
Published: December 21, 2012

 © 2012 American Chemical Society

N species, which results in a decrease in electron concentration with an increase of N content. Recently, high phosphorus concentrations and low resistivity in germanium have also been demonstrated using atomic layer doping technique by stacking multiple δ-doped layers.[16] In this study, the ZnO:N layer was prepared by the in situ atomic layer doping using the ALD technique. The nitrogen radicals were generated in remote NH_3/H_2 plasma and in situ incorporated into ZnO during the layer-by-layer growth. The nitrogen incorporation into ZnO effectively suppresses the electron concentration in ZnO and so gives rise to a decrease of the electron injection from *n*-ZnO:N to *p*-GaN:Mg layers, resulting in the dominant ultraviolet (UV) EL from ZnO in the *n*-ZnO:N/*p*-GaN:Mg heterojunction LEDs.

EXPERIMENTAL SECTION

The schematic of the *n*-ZnO:N/*p*-GaN:Mg heterojuncton LED is shown in Figure 1. First, a 30 nm GaN buffer layer, a 2.5 μm thick

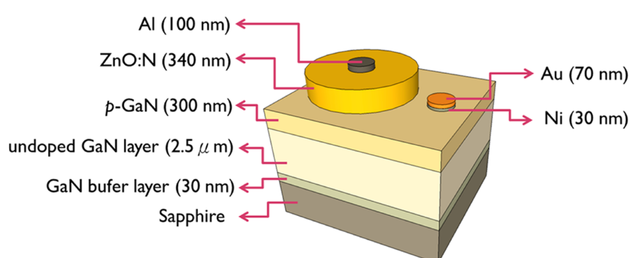

Figure 1. Schematic structure of the *n*-ZnO:N/*p*-GaN:Mg heterjunction LED.

undoped GaN layer, and a 300 nm Mg-doped GaN (GaN:Mg) layer were grown by metal−organic chemical vapor deposition (MOCVD) on a *c*-sapphire substrate. Then a ZnO:N film was grown upon the GaN:Mg layer by ALD (Fiji F202 Cambridge Nanotech) at a low temperature of 180 °C. Diethylzinc (DEZn, $Zn(C_2H_5)_2$), H_2O vapor, and NH_3 were utilized as the precursors for zinc, oxygen, and nitrogen, respectively, which were carried into the chamber with an Ar flow. The process consisted of two kinds of ALD cycles, the first contained the following sequence: DEZn → Ar purge → H_2O → Ar purge for the deposition of ZnO, and the second was DEZn → Ar purge → remote NH_3/H_2 plasma → Ar purge → H_2O → Ar purge for the in situ atomic layer doping of nitrogen into ZnO. A radio frequency (RF) coil with a power of 300 W was utilized to generate the remote NH_3/H_2 plasma. The nitrogen content in ZnO:N films can be precisely controlled by the number of atomic doped layers and their separation in the films.[15] In this study, one ALD cycle for the in situ atomic layer doping of nitrogen was carried out every 9 ZnO ALD cycles, i.e., the atomic layer doping percentage of nitrogen was 10%, for preparing the ZnO:N layer. The ALD cycles for atomic layer doping were uniformly distributed in total ALD cycles. The resulting ZnO:N film thickness was about 340 nm, which was confirmed by a spectroscopic ellipsometry. Subsequently, the ZnO:N/GaN:Mg structure was treated by rapid thermal annealing (RTA) at 1000 °C in oxygen atmosphere for 5 min to improve the crystalline quality as well as the uniformity of dopant distribution in the ZnO:N layer. Since oxygen vacancies in ZnO were considered as the donors in ZnO,[17] the oxygen atmosphere in the post-RTA treatment was used to reduce the density of oxygen vacancies. Afterward, a circular ZnO:N mesa of 1 mm in diameter was fabricated via the conventional lithography and the wet chemical etching by a very dilute HCl solution. Finally, Al and Ni/Au metal electrodes were deposited using thermal evaporation to form the Ohmic contacts on the ZnO:N and GaN:Mg layers, respectively.

The electrical characteristics of each layer were characterized by the Hall-effect measurement system (Ecopia HMS-3000) with the van der Pauw configuration. The X-ray photoelectron spectroscopy (XPS, PHI 5000 VersaProbe, ULVAC-PHI) was used to confirm the chemical state of nitrogen and determine the N content in the ZnO:N layer. The reference binding energy position was regulated by Au 4f 7/2 line at 84 eV. The photoluminescence (PL) spectroscopy was performed using a pulsed Q-switched diode-pumped solid-state laser (Advanced Optowave Corporation, wavelength = 266 nm, repetition rate =15 kHz) as an excitation source along with a monochromator (SpectroPro 2300i). The current−voltage characteristics (*I*−*V*) of the devices were measured using Keithley 2430 source meter.

RESULTS AND DISCUSSION

The XPS spectrum of the ZnO:N layer shown in Figure 2 reveals the N *1s* peak at ~399.2 eV associated with the Zn−N

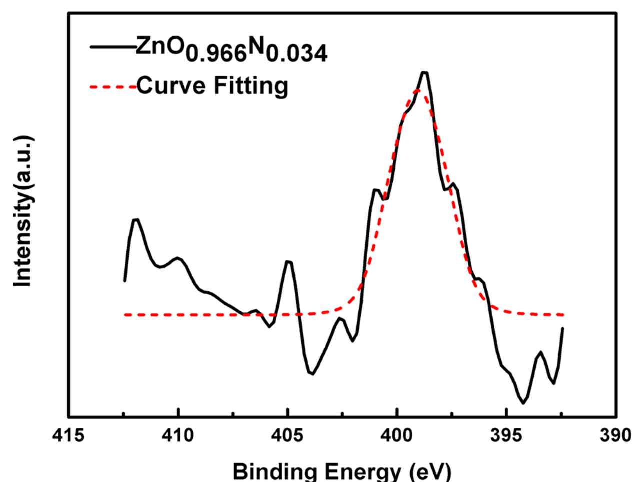

Figure 2. XPS spectrum of the ZnO:N layer, in which $ZnO_{0.966}N_{0.034}$ indicates the atomic compositions of O and N are 96.6% and 3.4%, respectively, given by the quantitative analysis on the XPS spectrum.

bond,[18,19] indicating the incorporation of nitrogen into ZnO layer as well as the substitution of N for O by the in situ atomic layer doping technique. The quantitative analysis on the XPS spectrum gives that the atomic compositions of O and N are 96.6% and 3.4%, as indicated by $ZnO_{0.966}N_{0.034}$ in Figure 2. The smaller atomic composition of N (3.4%) than the atomic layer doping percentage of nitrogen (10%) may result from the partial incorporation of nitrogen in each ALD cycle for in situ atomic layer doping. Because the remote NH_3/H_2 plasma was followed by the oxygen precursor (H_2O vapor) and the Zn−O bond is stronger than the Zn−N bond, the nitrogen incorporation in each ALD cycle for in situ atomic layer doping might be not a self-limiting process, which results in the partial incorporation of nitrogen.

Table 1 shows the conductivity type, carrier concentration, mobility, and resistivity of the ZnO (without the in situ atomic layer doping of nitrogen), ZnO:N, and GaN:Mg layers after the RTA treatment in oxygen atmosphere. Herein the ZnO-

Table 1. Electrical Properties of the ZnO (without N), ZnO:N, and GaN:Mg Layers after the RTA treatment in Oxygen Atmosphere

	majority carrier	concentration (cm^{-3})	mobility ($cm^2\ V^{-1}\ s^{-1}$)	resistivity (Ω cm)
ZnO (without N)	electron	3.04×10^{19}	24	0.0086
ZnO:N	electron	1.09×10^{18}	4.59	1.25
GaN:Mg	hole	7.39×10^{17}	6.15	0.7228

(without N) and ZnO:N films were grown on the *c*-sapphire substrate, using the same ALD condition as mentioned above. It can be clearly seen that the electron concentration decreases 1 order of magnitude, from 3.04×10^{19} cm^{-3} in the ZnO(without N) film to 1.09×10^{18} cm^{-3} in the ZnO:N layer. As seen in the XPS spectrum shown in Figure 2, the nitrogen-related acceptor states were introduced into ZnO by the in situ atomic layer doping process as a result of the occupation of O sites with N species. Therefore, the decrease in electron concentration may result from the compensation of the intrinsic donor states by the nitrogen-related acceptors.[15] The electron mobility decreases from 24 cm^2 V^{-1} s^{-1} for the ZnO(without N) film to 4.59 cm^2 V^{-1} s^{-1} for the ZnO:N layer, which can be explained by the formation of the impurity scattering centers due to the nitrogen incorporation.[20,21] It might be noted that the electron concentration was reduced by only 1 order of magnitude even though a large amount of nitrogen up to 3.4% was doped into ZnO. Since the remote NH_3/H_2 plasma was used in the in situ atomic layer doping process, the hydrogen may also be doped into the ZnO film. It is generally recognized that hydrogen behaves as a shallow donor in ZnO.[22] Therefore, the hydrogen incorporation may account for the decrease of only 1 order of magnitude in electron concentration despite a large amount of nitrogen incorporation into ZnO. On the other hand, the GaN:Mg layer exhibits a *p*-type conductivity with a hole concentration of 7.39 $\times 10^{17}$ cm^{-3} and mobility of 6.15 cm^2 V^{-1} s^{-1}, which were also listed in the Table 1.

For a comparison, Table 2 also shows the electron concentration, mobility, and resistivity of the ZnO:N films as

Table 2. Electron Concentration, Mobility, and Resistivity of the ZnO (without N) and ZnO:N Thin Films on *c*-Sapphire Substrates

	electron concentration (cm^{-3})	mobility (cm^2V^{-1} s^{-1})	resistivity (Ω cm)
ZnO	3.04×10^{19}	24	0.0086
$ZnO_{0.966}N_{0.034}$	1.09×10^{18}	4.59	1.25
$ZnO_{0.932}N_{0.068}$	3.44×10^{17}	4.43	3.67
$ZnO_{0.9}N_{0.1}$	1.03×10^{17}	2.31	20.05
$ZnO_{0.871}N_{0.129}$	6.30×10^{15}	1.03	724

a function of the N content. These ZnO:N films with various N contents were prepared on *c*-sapphire substrates also using the remote plasma in situ atomic layer doping technique. It is seen that the electron concentration decreases almost 4 orders of magnitude, from 3.04×10^{19} to 6.30×10^{15} cm^{-3}, with an increase of the N content from 0 to 0.129. Since the nitrogen incorporation into ZnO results in the formation of the N-related acceptors, the decrease in electron concentration can be mainly attributed to the compensation of the intrinsic donor states by the N-related acceptors.[22] It is also seen that the electron mobility decreases from 24 cm^2 V^{-1} s^{-1} for ZnO(without N) to 1.03 cm^2 V^{-1} s^{-1} for the $ZnO_{0.871}N_{0.129}$ film, also attributed to the formation of the impurity scattering centers associated with nitrogen.[20,21] Therefore, the significant decrease in the electron concentration and mobility, with an increase of the N content from 0 to 0.129, results in the dramatic increase of the resistivity from 0.0086 to 724 Ω cm, as shown in Table 2.

Figure 3a shows a conventional transmission electron microscopy (TEM) image of the *n*-ZnO:N/*p*-GaN:Mg

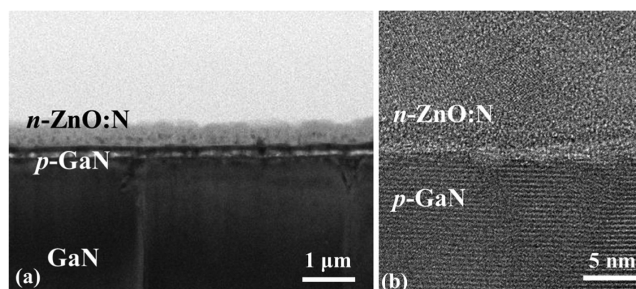

Figure 3. (a) Conventional TEM image of the postannealed *n*-ZnO:N/*p*-GaN:Mg films on the GaN layer. (b) High-resolution TEM image of an interface between the *n*-ZnO:N and *p*-GaN:Mg layers.

heterojunction on the GaN layer. In our previous investigation,[11] an *n*-ZnO(without N) film was prepared under almost the same ALD condition as the *n*-ZnO:N layer in this study, but without the in situ atomic layer doping of nitrogen. As seen in the TEM images in ref 11, the *n*-ZnO(without N) film grew in a good epitaxial relation with the GaN layer and to almost a perfect single crystal with very few dislocations. The threading dislocations from the underlying layers were reduced at the *n*-ZnO(without N)/*p*-GaN:Mg interface, mainly due to the layer-by-layer growth of ALD. A 4−5 nm ultrathin interfacial layer along the interface between the *n*-ZnO(without N) and *p*-GaN:Mg layers was formed due to the diffusion of Mg atoms from *p*-GaN:Mg into *n*-ZnO. It is evident that the structure of the *n*-ZnO:N layer is different from the *n*-ZnO(without N) film. The HRTEM image shown in Figure 3b reveals that the *n*-ZnO:N film may be regarded as mosaic crystals and the interfacial layer is not formed. From only a viewpoint of crystal growth of the *n*-ZnO:N layer, the postdeposition RTA treatment at 1000 °C for 5 min may be too short for nitrogen-doped ZnO to form a complete single-crystal film.

Figure 4 shows the normalized PL spectra of the postannealed ZnO:N and GaN:Mg layers at room temperature.

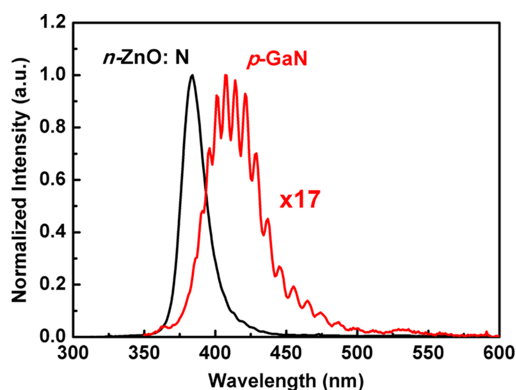

Figure 4. Normalized room-temperature PL spectra of the postannealed ZnO:N and GaN:Mg layers.

The ZnO:N layer exhibits a significant near band-edge emission at 383 nm, without defect-related band in the visible spectrum. In contrast, a broadband emission around 408 nm was observed in the PL spectrum from the GaN:Mg layer, which is attributable to the electron transitions from the conduction band or unidentified shallow donors to the Mg acceptor states.[23] The oscillating-like spectral peaks upon the PL spectrum from the GaN:Mg layer is caused by the interference

dx.doi.org/10.1021/am301799j | ACS Appl. Mater. Interfaces 2013, 5, 227−232

fringes because of the Fabry−Perot cavity between the air/GaN and GaN/sapphire interfaces.[24]

Figure 5 shows the $I-V$ characteristics of the n-ZnO(without N)/p-GaN:Mg and n-ZnO:N/p-GaN:Mg heterojunction LEDs

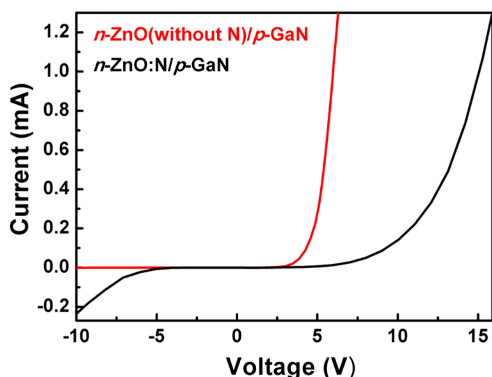

Figure 5. $I-V$ characteristics of the n-ZnO(without N)/p-GaN:Mg and n-ZnO:N/p-GaN:Mg heterojunction LED at room temperature.

at room temperature. Both devices exhibited rectifying, diode-like behavior. The n-ZnO(without N)/p-GaN:Mg device revealed larger forward-bias injection current and smaller reverse-bias leakage current than those of the n-ZnO:N/p-GaN:Mg heterojunction LED, attributed to the higher electron concentration in the n-ZnO(without N) film (3.04×10^{19} cm^{-3}) than that in the n-ZnO:N layer (1.09×10^{18} cm^{-3}). A lower majority carrier concentration in the ZnO:N layer may reduce the electron injection from n-ZnO:N to p-GaN:Mg, resulting in smaller forward-bias injection current and also larger reverse-bias leakage current in the n-ZnO:N/p-GaN:Mg heterojunction LED. Figure 6 displays the room-temperature

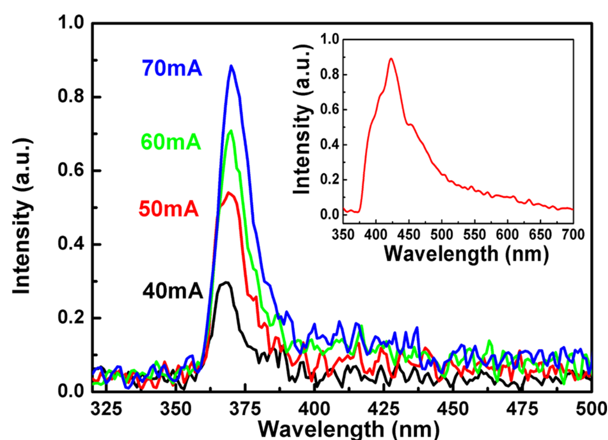

Figure 6. Room-temperature EL spectra of the n-ZnO:N/p-GaN:Mg heterojuntion LED at DC forward currents from 40 to 70 mA. Inset shows the EL spectrum of the n-ZnO(without N)/p-GaN:Mg heterojuntion LED.

EL spectra from the n-ZnO:N/p-GaN:Mg heterojuntion LED under the injection of DC forward currents from 40 mA to 70 mA. The device exhibits a dominant UV spectral peak centered at 370 nm and a very weak blue-violet emission around 415 nm. A comparison between these EL spectra and the PL spectra shown in Figure 4 indicates that the dominant EL peak at 370 nm may originate from the n-ZnO:N layer, and the small spectral envelope around 415 nm is attributed to the Mg acceptor levels in p-GaN:Mg. On the other hand, the inset in Figure 6 shows the EL spectrum from the n-ZnO(without N)/p-GaN:Mg heterojuntion LED at room temperature. A dominant spectral peak at 425 nm and a broad yellow band with a tail toward longer wavelength were observed in the EL spectrum from the n-ZnO(without N)/p-GaN:Mg heterojuntion LED, ascribed to the light emission from the Mg acceptor states[23] and the impurities or structural defects caused by the wet chemical etching in the p-GaN:Mg layer, respectively.[25]

The band alignment of the n-ZnO:N/p-GaN:Mg heterojunction was determined by the XPS technique. To analyze the valence band offset (ΔE_v) of the n-ZnO:N/p-GaN:Mg heterojunction, three samples were prepared: (i) bulk p-GaN:Mg, i.e. p-GaN:Mg(300 nm)/GaN(2.5 μm)/sapphire substrate, (ii) bulk n-ZnO:N, i.e., ZnO(340 nm)/p-GaN:Mg-(300 nm)/GaN(2.5 μm)/sapphire substrate, and (iii) the heterojunction interface, i.e. ZnO(7 nm)/p-GaN:Mg(300 nm)/GaN(2.5 μm)/sapphire substrate. The spectra were collected with a microfocused Al $K\alpha$ X-ray (25W, 100 μm). All XPS spectra were calibrated by C 1s peak at 284.60 eV from surface hydrocarbon contamination. The value of ΔE_v can be calculated using the method proposed by Wei and Deng[26,27]

$$\Delta E_v = \Delta E_{CL} + (E_{Ga2p}^{p-GaN:Mg} - E_{VBM}^{p-GaN:Mg}) - (E_{Zn2p}^{n-ZnO:N} - E_{VBM}^{n-ZnO:N}) \quad (1)$$

where $\Delta E_{CL} = (E_{Ga\ 2p}^{p\text{-GaN:Mg}} - E_{Ga\ 2p}^{n\text{-ZnO:N}})$ is the energy difference between Ga $2p_{3/2}$ and Zn $2p_{3/2}$ core levels (CLs) at the heterojunction interface, $(E_{Ga\ 2p}^{p-GaN:Mg} - E_{VBM}^{p\text{-GaN:Mg}})$ is the energy between Ga $2p_{3/2}$ and valence band maximum (VBM) in the bulk p-GaN:Mg, and $(E_{Zn\ 2p}^{n\text{-ZnO:}N} - E_{VBM}^{n\text{-ZnO:N}})$ is the energy between Zn $2p_{3/2}$ and valence band maximum (VBM) in the bulk of n-ZnO:N. Panels a and b in Figure 7 show that the core level spectra of Ga $2p_{3/2}$ (bulk p-GaN:Mg) and Zn $2p_{3/2}$ (bulk n-ZnO:N) are located at 1116.00 and 1021.10 eV, respectively. The valence band (VB) edge spectra of bulk p-GaN:Mg and bulk n-ZnO:N layers are shown in panels c and d in Figure 7, and the VBM of p-GaN:Mg and n-ZnO:N layers are 0.94 and 1.97 eV, respectively, as determined using a linear extrapolation method. Furthermore, the core levels of Ga $2p_{3/2}$ and Zn $2p_{3/2}$ at the heterojunction interface are determined to be 1116.50 and 1021.37 eV, as shown in panels e and f in Figure 7. According to eq 1 the ΔE_v value was calculated to be 0.8 eV, which agree well with the report from Hong.[28] Afterward, the conduction band offset ΔE_c could be calculated from $\Delta E_c = \Delta E_v + E_{g,ZnO} - E_{g,GaN}$, where the bandgap of ZnO ($E_{g,ZnO}$) and GaN ($E_{g,GaN}$) is 3.37 and 3.40 eV, respectively.[3] Thus the ΔE_c value is estimated to be 0.83 eV. As a result, a type II band alignment forms at the n-ZnO:N/p-GaN:Mg heterojunction as shown in Figure 8, where the conduction band and valence band offsets ΔE_c and ΔE_v are indicated.

Therefore, the energy barrier ΔE_v for hole injection from p-GaN:Mg into n-ZnO:N is smaller than energy barrier ΔE_c for electron injection from n-ZnO:N into p-GaN:Mg. However, as shown in Table 1, since the electron concentration in n-ZnO(without N) is 2 orders of magnitude greater than the hole concentration in p-GaN:Mg, the electron injection from n-ZnO(without N) into p-GaN:Mg is dominant over the hole injection from p-GaN:Mg into n-ZnO(without N). Accordingly, the EL of the n-ZnO(without N)/p-GaN:Mg LED mainly come from the p-GaN:Mg layer, as shown in the inset in Figure 6. In addition, as indicated in Table 1, the electron

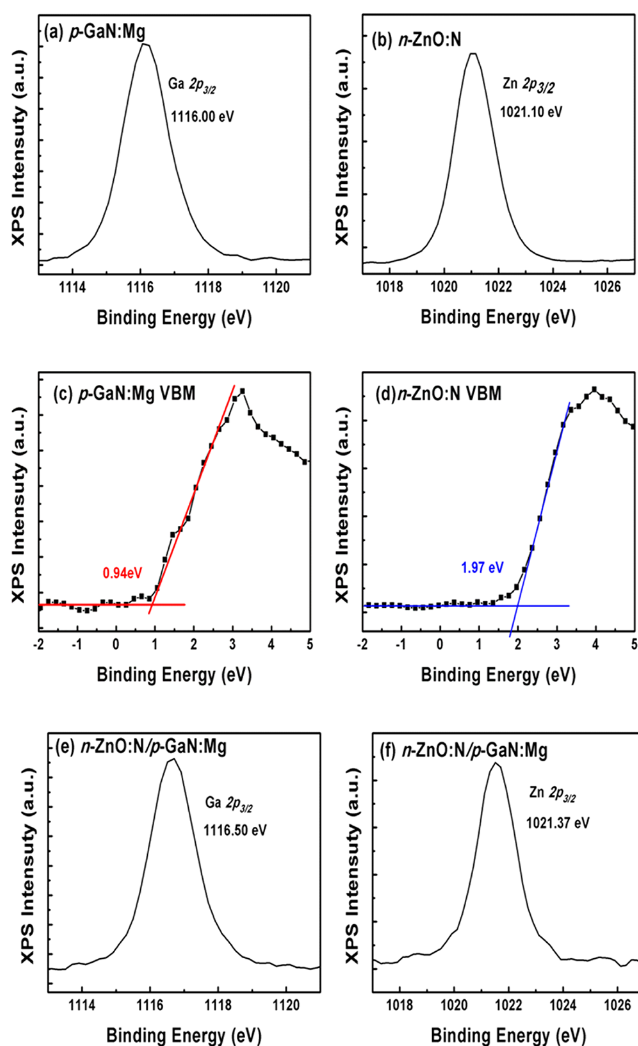

Figure 7. (a) CL of Ga $2p_{3/2}$ recorded on bulk *p*-GaN:Mg. (b) CL of Zn $2p_{3/2}$ recorded on bulk *n*-ZnO:N. (c, d) VB edge spectra of bulk *p*-GaN:Mg and bulk *n*-ZnO:N. (e, f) CL of *p*-GaN:Mg and *n*-ZnO:N at the *n*-ZnO:N/*p*-GaN:Mg interface.

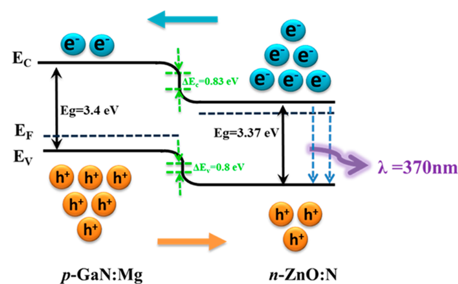

Figure 8. Band diagram of the *n*-ZnO:N/*p*-GaN:Mg heterojuntion under forward bias.

concentration in *n*-ZnO:N was effectively reduced to a value close to the hole concentration in *p*-GaN:Mg, due to the nitrogen incorporation into ZnO using the in situ atomic layer doping technique. Therefore, the hole injection from *p*-GaN:Mg into *n*-ZnO:N may prevail over the electron injection from *n*-ZnO:N into *p*-GaN:Mg because of the smaller energy barrier ΔE_v for holes than ΔE_c for electrons. As a result, the light emission from the ZnO:N layer dominates the EL spectra from the *n*-ZnO:N/*p*-GaN:Mg heterojunction LED, as demonstrated in Figure 6. The result indicates that the in situ atomic layer doping is an effective technique to incorporate nitrogen for reducing the electron concentration in ZnO.

■ CONCLUSIONS

The *n*-ZnO:N/*p*-GaN:Mg heterojunction LEDs have been fabricated by the growth of an *n*-type ZnO:N layer on *p*-type GaN:Mg, in which the nitrogen was incorporated into ZnO by the remote plasma in situ atomic layer doping technique. As compared with the ZnO(without N) layer, a significant decrease of electron concentration in the ZnO:N films was observed due to the formation of N-related acceptor states by the substitution of N for O sites, as indicated by the presence of Zn−N bond revealed by the XPS measurement. For the *n*-ZnO(without N)/*p*-GaN:Mg LED, the light emission mainly originate from the *p*-GaN:Mg layer due to the high electron concentration in the *n*-ZnO(without N) layer. The reduction in the electron concentration in the *n*-ZnO:N layer leads to a decrease in the electron injection from *n*-ZnO:N into *p*-GaN:Mg, yielding the dominant UV light emission from ZnO and the suppressed EL from GaN. Since the doping concentration can be precisely controlled by the number of atomic doped layers and their separation in the films, the results in this study demonstrates that the in situ atomic layer doping is an applicable technique to tailor the electrical properties of the materials for future applications in devices.

■ AUTHOR INFORMATION

Corresponding Author

*E-mail: mjchen@ntu.edu.tw.

Notes

The authors declare no competing financial interest.

■ ACKNOWLEDGMENTS

This work was supported in part by the National Science Council, Taipei, Taiwan, Republic of China, under Contract NSC 101-2120-M-002-010 and NSC 101-3113-E-002-009.

■ REFERENCES

(1) Alivov, Ya. I.; Look, D. C.; Ataev, B. M.; Chukichev, M. V.; Mamedov, V. V.; Zinenko, V. I.; Agafonov, Yu. A.; Pustovit, A. N. *Solid-State Electron.* **2004**, *48*, 2343.
(2) Chen, Y.; Bagnall, D.; Yao, T. *Mater. Sci. Eng., B* **2000**, *75*, 190−198.
(3) Jiao, S. J.; Lu, Y. M.; Shen, D. Z.; Zhang, Z. Z.; Li, B. H.; Zhang, J. Y.; Yao, B.; Liu, Y. C.; Fan, X. W. *Phys. Status Solidi (c)* **2006**, *3*, 972.
(4) You, J. B.; Zhang, X. W.; Zhang, S. G.; Wang, J. X.; Yin, Z. G.; Tan, H. R.; Zhang, W. J.; Chu, P. K.; Cui, B.; Wowchak, A. M.; Dabiran, A. M.; Chow, P. P. *Appl. Phys. Lett.* **2010**, *96*, 201102.
(5) Lee, J. Y.; Lee, J. H.; Kim, H. S.; Lee, C. H.; Ahn, H. S.; Cho, H. K.; Kim, Y. Y.; Kong, B. H.; Lee, H. S. *Thin Solid Films* **2009**, *517*, 5157−5160.
(6) Sun, J. C.; Liang, H. W.; Zhao, J. Z.; Bian, J. M.; Feng, Q. J.; Hu, L. Z.; Zhang, H. Q.; Liang, X. P.; Luo, Y. M.; Du, G. T. *Chem. Phys. Lett.* **2008**, *460*, 548−551.
(7) Yang, T. P.; Zhu, H. C.; Bian, J. M.; Sun, J. C.; Dong, X.; Zhang, B. L.; Liang, H. W.; Li, X. P.; Cui, Y. G.; Du, G. T. *Mater. Res. Bull.* **2008**, *43*, 3614−3620.
(8) Bayram, C.; Hosseini Teherani, F.; Rogers, D. J.; Razeghi, M. *Appl. Phys. Lett.* **2008**, *93*, 081111.
(9) Rogers, D. J.; Hosseini Teherani, F.; Yasan, A.; Minder, K.; Kung, P.; Razeghi, M. *Appl. Phys. Lett.* **2006**, *88*, 141918.

(10) Wu, M. K.; Shih, Y. T.; Li, W. C.; Chen, H. C.; Chen, M. J.; Kuan, H.; Yang, J. R.; Shiojiri, M. *IEEE Photonic Tech. Lett.* **2008**, *20*, No. 2.
(11) Chen, H. C.; Chen, M. J.; Wu, M. K.; Li, W. C.; Tsai, H. L.; Yang, J. R.; Kuan, H.; Shiojiri, M. *IEEE J. Quantum Electron.* **2010**, *46*, No. 2.
(12) Alivov, Ya. I.; Van Nostrand, J. E.; Look, D. C.; Chukichev, M. V.; Ataev, B. M. *Appl. Phys. Lett.* **2003**, *83*, 2943.
(13) Xu, H. Y.; Liu, Y. C.; Liu, Y. X.; Xu, C. S.; Shao, C. L.; Mu, R. *Appl. Phys. B: Laser Opt.* **2005**, *80*, 871−874.
(14) Chuang, R. W.; Wu, R. X.; Lai, L. W.; Lee, C. T. *Appl. Phys. Lett.* **2007**, *91*, 231113−1−231113−3.
(15) Chien, J. F.; Chen, C. H.; Shyue, J. J.; Chen, M. J. *ACS Appl. Mater. Interfaces* **2012**, *4*, 3471−3475.
(16) Scappucci, G.; Capellini, G.; Klesse, W. M.; Simmons, M. Y. *Nanotechnology* **2011**, *22*, 375203.
(17) Shih, Y. T.; Chien, J. F.; Chen, M. J.; Yang, J. R.; Shiojiri, M. *J. Electrochem. Soc.* **2011**, *158* (5), 516−H520.
(18) Hsieh, H. H.; Wu, C. C. *Appl. Phys. Lett.* **2007**, *91*, 013502.
(19) Joseph, M.; Tabata, H.; Saeki, H.; Ueda, K.; Kawai, T. *Physica B* **2001**, *302*−*303*, 140.
(20) Lu, J.; Zhang, Y.; Ye, Z.; Wang, L.; Zhao, B.; Huang, J. *Mater. Lett.* **2003**, *57*, 3311.
(21) Lim, S. J.; Kwon, S.; Kim, H.; Park, J. S. *Appl. Phys. Lett.* **2007**, *91*, 183517.
(22) Dutta, M.; Ghosh, T.; Basak, D. *J. Electron. Mater.* **2009**, *38*, 2335−2342.
(23) Xu, H. Y.; Liu, Y. C.; Liu, Y. X.; Xu, C. S.; Shao, C. L.; Mu, R. *Appl. Phys. B: Laser Opt.* **2005**, *80*, 871−874.
(24) Billeb, A.; Grieshaber, W.; Stocker, D.; Schubert, E. F.; Karlicek, R. F., Jr. *Appl. Phys. Lett.* **1997**, *70*, 21.
(25) Basak, D.; Lachab, M.; Nakanishi, T.; Sakai, S. *Appl. Phys. Lett.* **1999**, *75*, 3710.
(26) Wei, S. H.; Zunger, A. *Appl. Phys. Lett.* **1998**, *72*, 2011.
(27) Deng, R.; Yao, B.; Li, Y. F.; Zhao, Y. M.; Li, H.; Shan, C. X.; Zhang, Z. Z.; Zhao, D. X.; Zhang, J. Y.; Shen, D. Z.; Fan, X. W. *Appl. Phys. Lett.* **2009**, *94*, 022108.
(28) Hong, S. K.; Hanada, T.; Makino, H.; Chen, Y.; Ko, H. J. *Appl. Phys. Lett.* **2001**, *78*, 3349.